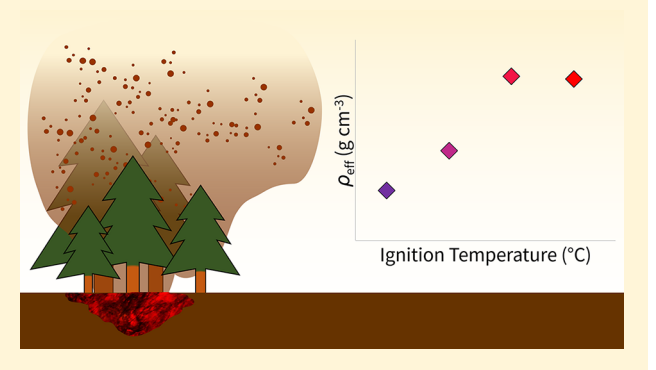


Density and Homogeneous Internal Composition of Primary Brown **Carbon Aerosol**

Benjamin J. Sumlin, †, § Christopher R. Oxford, †, § Bongjin Seo, † Robert R. Pattison, † Brent J. Williams, † and Rajan K. Chakrabarty*, To

Supporting Information

ABSTRACT: The presence of atmospheric brown carbon (BrC) has been the focus of many recent studies. These particles, predominantly emitted from smoldering biomass burning, absorb light in the near-ultraviolet and short visible wavelengths and offset the radiative cooling effects associated with organic aerosols. Particle density dictates their transport properties and is an important parameter in climate models and aerosol instrumentation algorithms, but our knowledge of this particle property is limited, especially as functions of combustion temperature and fuel type. We measured the effective density (ρ_{eff}) and optical properties of primary BrC aerosol emitted from smoldering combustion of Boreal peatlands. Energy transfer into the fuel was controlled by selectively altering the combustion ignition temper-



ature, and we find that the particle $\rho_{\rm eff}$ ranged from 0.85 to 1.19 g cm⁻³ corresponding to ignition temperatures from 180 to 360 °C. BrC particles exhibited spherical morphology and a constant 3.0 mass-mobility exponent, indicating no internal microstructure or void spaces. Upon partial thermal volatilization, ρ_{eff} of the remaining particle mass was confined to a narrow range between 0.9 and 1.1 g cm⁻³. These findings lead us to conclude that primary BrC aerosols from biomass burning have homogeneous internal composition, and their ρ_{eff} is in fact their actual density.

1. INTRODUCTION

The density of a particle is an important physical property for understanding and parametrizing its transport properties in the atmosphere and the human respiratory system.¹ It also influences the particle optical properties, since the indices of refraction tend to increase with increasing density.2 The first determinations of density were made for homogeneous spherical particles from measurements of their mass (m_p) and electrical mobility diameters $(d_{\rm m})$ using a Millikan cell. In the case where the particles deviate from spherical morphology and homogeneous composition, the dynamic shape factor must be included when relating the aerodynamic and mobility diameters. This dimensionless parameter accounts for the effect of nonsphericity on the particle drag force. It is difficult to accurately measure the dynamic shape factor for single particles, so an alternative particle property, the effective density (ρ_{eff}) , has been adopted by the atmospheric aerosol community, primarily due to the recent advancement in aerosol instrumentation technologies for measuring this parameter.^{4–8} The $\rho_{\rm eff}$ of a particle is defined as^{4,5}

$$\rho_{\text{eff}} = \frac{6m_{\text{p}}}{\pi d_{\text{m}}^3} \tag{1}$$

The relationship between $d_{\rm m}$ and $m_{\rm p}$ can also be formulated as a power law expression: 10,11

$$m_{\rm p} = C d_{\rm m}^{D_{\rm m}} \tag{2}$$

where $D_{\rm m}$ is the mass-mobility exponent and C is a prefactor. Combining eqs 1 and 2, the expression for ρ_{eff} becomes ¹²

$$\rho_{\text{eff}} = \frac{6Cd_{\text{m}}^{D_{\text{m}}}}{\pi d_{\text{m}}^{3}} = Kd_{\text{m}}^{D_{\text{m}}-3} \tag{3}$$

where K ($K = 6C/\pi$) is a constant.^{9,13} For a homogeneous spherical particle with $D_{\rm m} \approx$ 3, its $\rho_{\rm eff}$ will be constant per eq 3. However, in cases where a particle is not spherical or has internal void spaces, ρ_{eff} will decrease with increasing size. McMurry et al. utilized eq 3 to calculate the actual density of spherical liquid particles using a combination of an electrostatic classifier and an aerosol particle mass analyzer. 12 Olfert and Collings introduced the centrifugal particle mass analyzer

January 6, 2018 Received: Revised: February 26, 2018 Accepted: March 1, 2018 Published: March 1, 2018

Department of Energy, Environmental and Chemical Engineering, Washington University in St Louis, St Louis, Missouri 63130, United States

[‡]United States Forest Service, Pacific Northwest Research Station, Anchorage, Alaska 99501, United States

(CPMA) to measure single particle mass, ¹⁴ and used this instrument to determine the $\rho_{\rm eff}$ of soot particles emitted from various sources. ^{7–9,13,15}

Primary BrC particles are a major component of emissions from the low-temperature, flameless smoldering phase of combustion of solid biomass fuels, such as peatland and duff. Peat constitutes the organic soil in wetlands made of partially decayed plant remains, and carbon accumulation in this ground-layer biomass has been occurring over hundreds to thousands of years. Smoldering combustion of this ground-layer biomass during the past several decades in the boreal and Arctic regions has received attention in recent times for contributing to rapid global climate change. 20–23

Brown carbon (BrC) aerosols have been recently identified as a major component of light absorbing carbonaceous matter in the atmosphere. These particles derive their name from their strong absorption of solar radiation in the ultraviolet to near visible spectrum which imparts a brownish appearance. $^{30-33}$

Humic-like substances (HULIS), produced from oligomerization of water-soluble organics and multiphase chemistry of organic constituents emitted from anthropogenic and natural sources such as biomass burning and vehicle exhaust, have been identified as an important constituent of BrC aerosols.³⁴ These particles occur in distinctive spherical shapes and are amorphous in composition with no internal microstructure, such as graphene-like layers found in soot.^{17,35} When observed under vacuum conditions by an electron microscope, loss of volatile matter is rarely observed from these particles.³⁵ This can be attributed to low-volatility, high molecular weight compounds constituting the bulk composition of these aerosols.³⁴

Very little research has been done on the $ho_{ ext{eff}}$ of primary BrC aerosols. Previous investigations have primarily focused on estimating the density of highly oxygenated HULIS extracts from atmospheric aerosols. Dinar et al. measured the $ho_{
m eff}$ of HULIS isolated from atmospheric aerosols, as well as fulvic acid (FA) and humic acid (HA) samples from aquatic and terrestrial sources.³⁶ They aerosolized the extract solutions and calculated $\rho_{\rm eff}$ of the aerosols by comparing the $d_{\rm m}$ and vacuum aerodynamic diameters and reported a range of $\rho_{
m eff}$ between 1.47 and 1.72 g cm⁻³. Hoffer et al. measured the $\rho_{\rm eff}$ of HULIS extracted from smoke and pollution aerosol particles sampled as part of the Large Scale Biosphere Atmosphere Experiment in Amazonia-Smoke Aerosols, Clouds, Rainfall, and Climate (LBA-SMOCC) experiment in 2002.³⁷ They reported $\rho_{\rm eff}$ values in the range of 1.50-1.57 g cm⁻³, consistent with Dinar et al.

In this study, we performed laboratory-scale smoldering experiments on Alaskan peat samples to generate primary BrC aerosols and measured their $\rho_{\rm eff}$ as a function of varying combustion conditions. Our approach differs from previous studies that reaerosolized solvent extracts of the original aerosol. Our method analyzes the original aerosol, and is fully inclusive of all chemical components. We also investigated the variation in $\rho_{\rm eff}$ upon partial thermal volatilization of the organic matter constituting these particles. We anticipate results from this study to find use in chemical transport models ^{29,38,39} and the data analysis algorithms associated with contemporary aerosol instruments such as aerosol mass spectrometers and electrical low pressure impactors. ^{5,6,40,41} Additionally, we obtained in situ real-time, contact-free measurements of the aerosol light absorption and light scattering coefficients to

contribute to the growing knowledge base of BrC optical properties. Since the chemical speciation of BrC is highly variable, so are its optical properties. The Constraining the effective complex refractive index (m = n + ik) has been a challenge for the atmospheric aerosol community, and such research is useful for climate modeling and satellite retrieval algorithms.

2. MATERIALS AND METHODS

2.1. Aerosol Generation. Figure 1 shows the schematic diagram of our experimental set up in this study. BrC particles

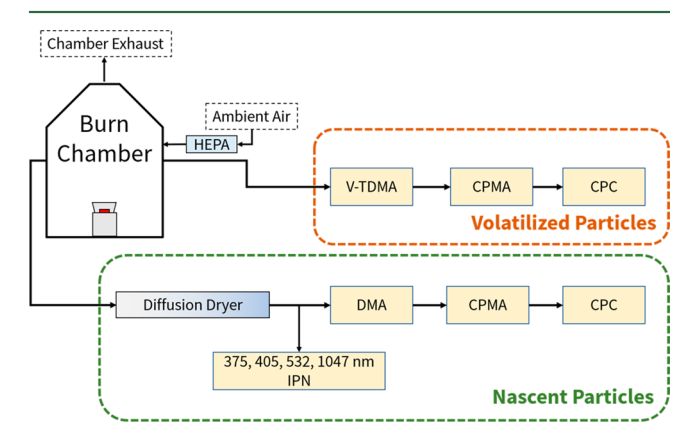


Figure 1. Schematic diagram of the experimental setup. Dashed-line bounding boxes indicate the separate sets of experiments. The green box indicates the setup for measurements of nascent brown carbon (BrC) particles, and the orange box indicates the setup for volatilized particles.

were generated from smoldering combustion of Alaskan peat soil samples at ignition temperatures of 180, 220, 240, 260, 300, and 360 °C. The peat was dried in a laboratory room with 50% relative humidity, and samples were combusted in a sealed 21 m³ stainless steel chamber equipped with a computercontrolled sample heater and recirculation fan. The chamber is grounded and electrically neutral, mitigating the effects of electrostatic wall losses. The large volume of the chamber mitigates some diffusional losses. Thin layers of 5-10 g of peat were evenly distributed on a rectangular stainless steel plate and heated to the desired temperature by a ring heater with a thermocouple to monitor the ignition temperature and close the control loop. It is important to note that the temperatures we report are not the actual combustion temperature, but rather the temperature of the heating element. Biomass smoldering is a highly exothermic process and the actual combustion temperature is much higher. Peat usually burns in stratified layers, and the temperature of the hot plate is a proxy for the temperature of an adjacent fuel layer, and a measure of energy transfer into the fuel.42

Prior to $\rho_{\rm eff}$ measurements, we measured the size distributions of BrC aerosols using a scanning mobility particle sizer (SMPS; TSI Inc., Model 3938) to track the temporal evolution of particle number size distributions. We determined that the distributions reached their steady-state conditions typically about 20 min after the start of a burn, with the majority of particles released within 5 min of initial smoke. We allowed the smoke to mix and began $\rho_{\rm eff}$ measurements 30 min after ignition

2.2. Effective Density, Optical Properties, And Elemental Composition of Nascent Particles. The $\rho_{\rm eff}$ of

nascent BrC particles was measured using a differential mobility analyzer (DMA; TSI Inc., model 3082), a CPMA (Cambustion Ltd.), and a condensation particle counter (CPC; TSI Inc., model 3787) in series, as shown in Figure 1. The particles were sampled through a diffusion dryer situated between the biomass burning chamber and the DMA to reduce the water vapor content in the flow stream to less than 15%. The DMA selected monodisperse particles based on their $d_{\rm m}$, and the particles were classified by the CPMA as a function of $m_{\rm p}$. The $\rho_{\rm eff}$ and mass-mobility relationship were calculated by using eqs 1 and 2.

To measure BrC absorption and scattering coefficients (β_{abs} and β_{sca} , respectively), we used four integrated photoacousticnephelometer (IPN) spectrometers operating at wavelengths (λ) of 375, 405, 532, and 1047 nm. ¹⁶ These instruments are of our own design and construction and are discussed in the Supporting Information (SI). PyMieScatt, a highly visual, opensource Lorenz-Mie theory inversion package was used to calculate the effective complex refractive indices (m = n + ik)from the scattering and absorption coefficients and number size distribution data. 44 Size distributions were corrected by total number concentration, since the usual SMPS units of dN/dlogd_n introduce significant errors in the retrievals. Due to scattering measurement miscalibrations, only the absorption data was available to infer m. However, using PyMieScatt's visual inversion algorithms along with literature data, we were able to constrain the possible values of both the real (n) and imaginary (k) parts of m by using previously reported values of n to identify a narrow range of k values.

The elemental composition of BrC aerosols was analyzed using X-ray photoelectron spectroscopy (XPS; Physical Electronics Inc., model 5000 VersaProbe II Scanning ESCA) to compare the composition of our laboratory aerosols with those observed in field studies.

2.3. Effective Density of Partially Volatilized Particles. Partially volatilized BrC particles were analyzed for their ρ_{eff} using a volatility tandem differential mobility analyzer (V-TDMA), which consists of two DMAs (TSI Inc., model 3081) separated by a heating section, shown in Figure 1.45,46 In the V-TDMA, the first DMA selected 200 nm monodisperse BrC aerosols, which were subsequently volatilized in the heating section. The second DMA scanned the resulting size distribution and then selected the $d_{\rm m}$ corresponding to the peak number concentration after volatilization. The average residence time in the heating section was 9.7 s, and particles sampled from the burn chamber were volatilized at internal temperatures of 60, 120, and 250 °C by the V-TDMA. These temperatures were chosen based on the results of our preliminary study (SI Figure S1). After leaving the heating section, particles cooled to ambient temperature (~23 °C) before classification by DMA 2. The m_p for the volatilized particles was measured using the CPMA and CPC, and the $\rho_{\rm eff}$ was calculated as described above.

3. RESULTS AND DISCUSSION

3.1. Optical Properties, Chemical Composition, And Size Distributions of Nascent BrC. Figure 2 shows the time-averaged β_{abs} measured by the IPN systems for particles emitted at smoldering ignition temperatures of 220 and 300 °C. We observed strong absorption at the near-ultraviolet wavelengths compared to absorption at 532 and 1047 nm, an indicator of BrC. 16,31,33 From these measurements, we used PyMieScatt to infer the effective complex refractive index m = n + ik. Figure 3

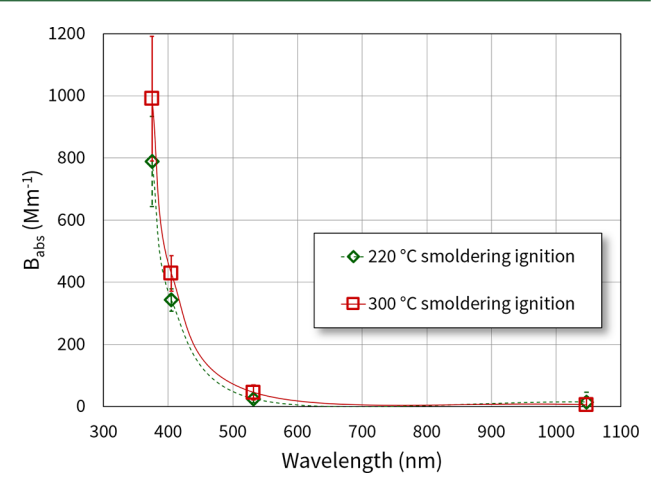


Figure 2. Light absorption coefficient (β_{abs}) of brown carbon (BrC) aerosols measured by the integrated photoacoustic-nephelometer spectrometers at four wavelengths. The strong absorption in the near-UV wavelengths is a defining characteristic for BrC aerosols. Error bars represent one standard deviation.

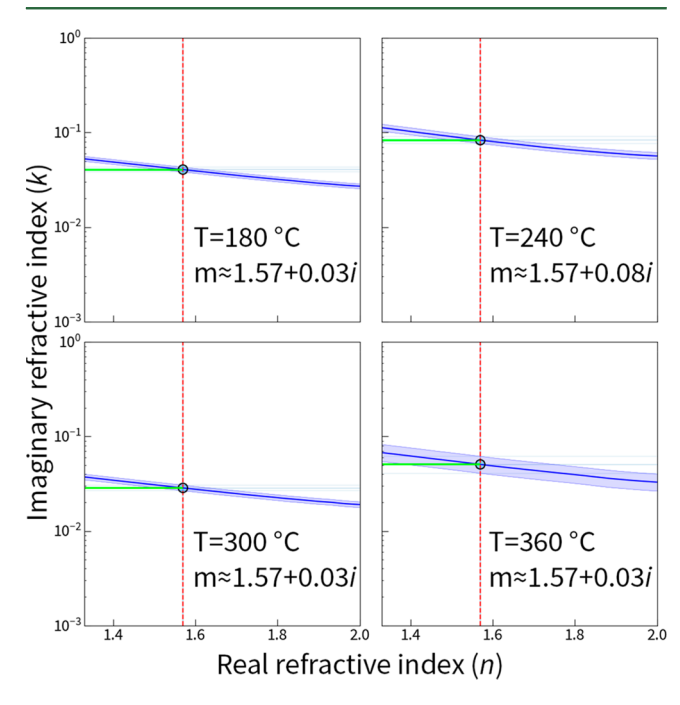


Figure 3. Complex refractive indices at $\lambda = 405$ nm for peat BrC aerosol generated from combustion ignition temperatures of 180, 240, 300, and 360 °C. The blue contour represents absorption measurements from this study, and the red line is an assumed real part of 1.57 based on previous studies. The intersection represents the effective complex m, and from this intersection we can infer the imaginary part k (green line). Errors in the retrievals are given in Table 1.

shows our inference of 405 nm m using absorption measurements from this study and an assumed real part of 1.57 from previous studies that used similar BrC generation methods. Since polydisperse distributions generally do not exhibit multiple solutions to their Lorenz-Mie inversions, we are confident in the validity of the retrievals. Values of all retrievals are given in Table 1, along with absorption Ångström exponents (AÅE) calculated from the two-wavelength formula:

Table 1. Retrieved Approximate Imaginary Refractive Indices (k) and Absorption Ångström Exponents Across $\lambda = 375$, 405, 532, 1047 nm from BrC Aerosol Emitted from Peat Ignited at 180, 240, 300, and 360 °C^a

	180 °C	240 °C	300 °C	360 °C		
wavelength, assumed n	k from different ignition temperatures					
375 nm, $n = 1.59 - 1.68$	$0.07 \pm 0.02 - 0.08 \pm 0.01$	0.41 ± 0.19	$0.05 \pm 0.01 - 0.06 \pm 0.01$	$0.09^{+0.07}_{-0.04}$ - $0.10^{+0.08}_{-0.04}$		
405 nm, n = 1.57	0.04 ± 0.00	0.08 ± 0.01	0.03 ± 0.00	0.03 ± 0.01		
532 nm, $n = 1.46 - 1.52$	0.02 ± 0.00	0.03 ± 0.00	0.01 ± 0.00	0.01 ± 0.00		
1047 nm, $n = 1.54 - 1.59$	0.03 ± 0.00	0.06 ± 0.01	0.03 ± 0.01	0.03 ± 0.01		
wavelength range	absorption Ångström exponents					
375-405 nm	$7.36^{+1.49}_{-1.46}$	$7.36^{+1.36}_{-1.70}$	$7.41^{+0.11}_{-0.09}$	6.40 ± 3.34		
405-532 nm	3.98 ± 0.03	4.09 ± 0.02	$4.41^{+0.11}_{-0.09}$	4.47 ± 0.27		
532-1047 nm	$0.50^{+0.14}_{-0.12}$	$0.22^{+0.16}_{-0.17}$	0.24 ± 0.01	0.62 ± 0.33		

"Where applicable for k, a range is reported. For these retrievals, the real refractive index n was assumed using literature data from similar experiments. ^{47,48} The assumed value or range is denoted under the wavelength in the left column. Errors are from propagation of standard deviations in β_{abs} through the calculations.

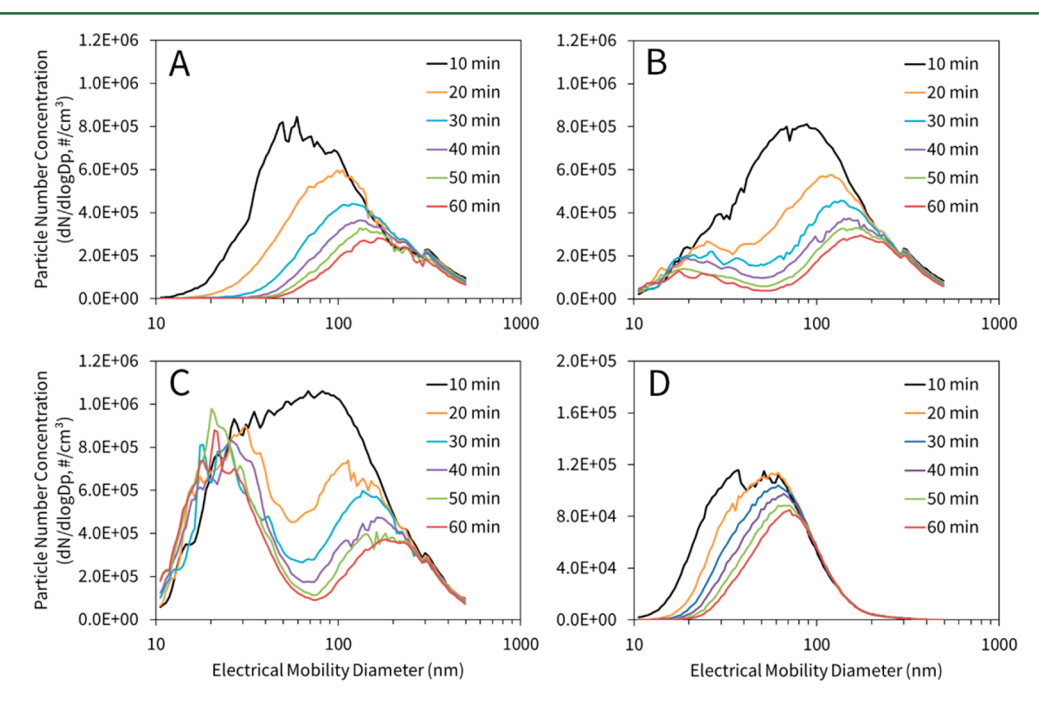


Figure 4. Number size distributions of BrC aerosols and their evolution at smoldering ignition temperatures of A: 180 $^{\circ}$ C; B: 240 $^{\circ}$ C; C: 300 $^{\circ}$ C; and D: 360 $^{\circ}$ C.

$$A\dot{A}E(\lambda_1, \lambda_2) = -\frac{\ln\left[\frac{\beta_{\text{abs}}(\lambda_1)}{\beta_{\text{abs}}(\lambda_2)}\right]}{\ln\left[\frac{\lambda_1}{\lambda_2}\right]}$$
(4)

Visualization of all retrievals are included in the SI. Across all ignition temperatures, the trend in k decreases with increasing wavelength. As functions of temperature, we observe that k trends slightly higher for BrC generated at 240 °C ignition.

XPS analysis of these particles shows an average carbon to oxygen (C:O) atomic ratio of 12:1 (SI Figure S2), which is on the higher side of the range observed for atmospheric tar balls, a specific type of BrC.^{50–53} Possible reasons for this discrepancy could be the use of a different technique, viz. electron dispersive spectroscopy (EDS) for measuring the C:O ratio, or that XPS analysis shows only the elemental composition of the particle surface, not the bulk.

Figure 4 shows SMPS measurements of the temporal evolution of the number size distributions of BrC aerosol particles emitted from smoldering ignition temperatures of 180,

240, 300, and 360 °C. The number concentrations corresponding to 300 °C were generally around five times higher than at 180 °C, indicating that more rapid energy transfer into the fuel layer creates combustion products, while lower energy transfer rates may favor volatization products. As expected for a closed system, the number concentrations decreased and geometric mean $d_{\rm m}$ increased with increasing particle residence time in the chamber. These rates were driven by diffusional losses and are subject to the particle concentration, which varied with ignition temperature. For example, the peak number concentrations of particles from the ignition temperature of 180 °C decreased slowly from approximately 1.2×10^5 to 8.0×10^4 cm⁻³ in a span of 60 min (a 33% reduction), while those corresponding to temperatures of over 240 °C showed a rapid decrease from approximately 1.0×10^6 to 3.0×10^5 cm⁻³ (a 70% reduction). The mean diameter values for particles corresponding to the four smoldering temperatures were initially 40-70 nm, and then increased to between 70 and 160 nm within 60 min in the burn chamber.

For combustion ignition temperatures between 300 and 360 °C, the number size distributions showed a distinct bimodal behavior with nucleation and accumulation modes. The nucleation mode distribution tapered off at approximately 40 nm, and its peak decreased with time as smaller particles diffuse more rapidly than larger particles, which scavenge smaller ones more efficiently. The accumulation mode consisted of particles ranging between 50 and 500 nm in d_m . Even though the number size distributions for the BrC aerosols generated at over 240 °C simultaneously showed both the nucleation and accumulation modes, we size-selected only accumulation mode particles larger than $d_m = 50$ nm for our $\rho_{\rm eff}$ measurements.

3.2. Effective Density and Mass-Mobility Relationship of Nascent Aerosol. Figure 5 shows the $\rho_{\rm eff}$ of nascent BrC

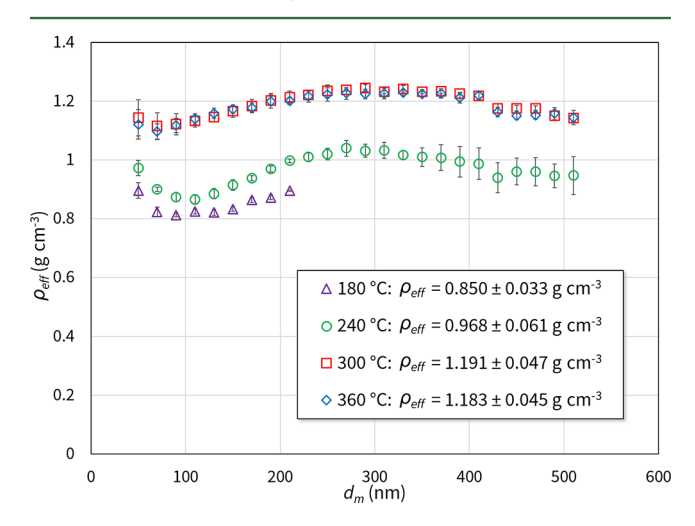


Figure 5. Effective densities ($\rho_{\rm eff}$) of nascent BrC aerosols, emitted at ignition temperatures of 180, 240, 300, and 360 °C, as a function of their mobility diameter ($d_{\rm m}$). Values are averages from three replicate experiments and error bars represent one standard deviation.

aerosols emitted from smoldering combustion at different temperatures, plotted as a function of their $d_{\rm m}$. For nonspherical particles, the $\rho_{\rm eff}$ tends to decrease with increasing $d_{\rm m}$. However, the magnitude of $\rho_{\rm eff}$ measured in our study was nearly constant for all $d_{\rm m}$, but it varied with ignition temperatures. This suggests that with higher rates of energy transfer into the fuel bed, emitted particles will contain denser constituents. This is consistent with the observation above that a higher ignition temperature will preferentially emit smoldering products rather than lightweight volatilization products. This observation agrees with previous findings that place the onset of peat pyrolysis at ignition temperatures between 250 and 300 °C. 19,59 We find that the average $\rho_{\rm eff}$ of 0.85 \pm 0.03 and 0.97 ± 0.05 g cm⁻³ for the particles generated at 180 and 240 °C smoldering temperatures were clearly lower than those of 1.19 \pm 0.04 and 1.18 \pm 0.04 g cm⁻³ for the particles generated at 300 and 360 °C. The average ρ_{eff} of BrC generated at over 300 °C is smaller than the reported $ho_{
m eff}$ values of 1.47– 1.72 g cm⁻³ for HULIS, FA, and HA.^{36,37}

Figure 6 shows the mass-mobility exponent $D_{\rm m}$ of BrC aerosol at various combustion ignition temperatures, calculated as the slope of the linear regression of $m_{\rm p}(d_{\rm m})$ in log-log space. The $D_{\rm m}$ values for these experiments is a constant value of 3.0 regardless of ignition temperature, indicating that the particles are homogeneous and free of internal voids. Indeed, electron microscopy of particles gathered during this study show a

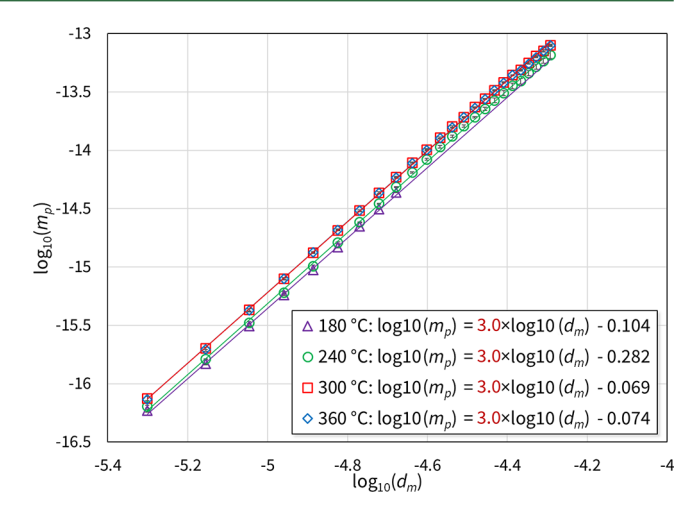


Figure 6. Calculation of the mass-mobility exponents $D_{\rm m}$ of nascent BrC aerosols. $D_{\rm m}$ is the slope of the linear regression in log–log space, and for all ignition temperatures the value was 3.0. Values are averages from three replicate experiments and error bars represent one standard deviation.

nearly spherical, homogeneous morphology (see SI Figure S3). It is therefore likely that these particles belong to the tar ball subset of BrC aerosols. High carbon—oxygen molar ratios of these particles as measured by XPS analysis further corroborates this hypothesis. The spherical morphology, along with the constant $D_{\rm m}$ of 3.0, leads us to conclude that the $\rho_{\rm eff}$ of these particles is in fact their true density.

3.3. Effective Density and Mass Fraction Remaining of Thermally Volatilized Aerosol. Figure 7 shows the average $\rho_{\rm eff}$ and mass fractions remaining (MFR) of BrC aerosols after partial volatilization by the V-TDMA. Table 2 summarizes the average values and standard deviations of measured $\rho_{\rm eff}$ as a function of temperature inside the heating section of the V-TDMA. When heated in the V-TDMA, the particle mass remaining after thermal volatilization showed a higher average

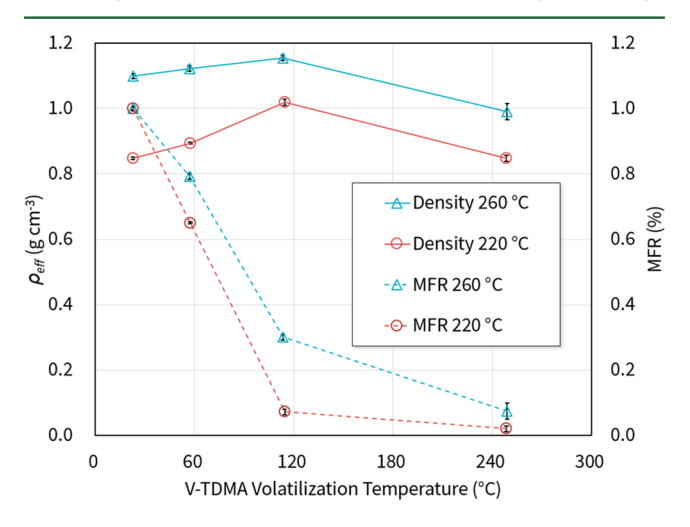


Figure 7. Average effective densities ($\rho_{\rm eff}$) and average mass fractions remaining (MFR) of BrC aerosols as a function of heating temperature in the volatility tandem differential mobility analyzer (V-TDMA). The circles and triangles correspond to combustion ignition temperatures of 220 and 260 °C, respectively. Dashed lines connect the MFR values, while the solid lines connect the measured $\rho_{\rm eff}$ of the devolatilized particle mass. Values are averages from five replicate experiments (four for 249 °C) and error bars represent one standard deviation.

Table 2. Average $\rho_{\rm eff}$ and MFR of Volatilized BrC Aerosols As a Function of Heating Temperature in the Volatility Tandem Differential Mobility Analyzer (V-TDMA).^a 220 and 260 °C are the Combustion Ignition Temperatures

	220 °C		260 °C	
heating temperature inside V-TDMA	$\rho_{\rm eff}$ (g cm ⁻³)	MFR	$\rho_{\rm eff}$ (g cm ⁻³)	MFR
23 °C (room temperature)	0.85 ± 0.00	1.00	1.10 ± 0.01	1.00
60 °C	0.89 ± 0.00	0.65	1.12 ± 0.01	0.79
120 °C	1.02 ± 0.01	0.07	1.15 ± 0.01	0.30
250 °C	0.85 ± 0.01	0.02	0.99 ± 0.03	0.07
average	0.90 ± 0.00		1.10 ± 0.02	

 $[^]a\mathrm{The}$ values reported for ρ_{eff} also include the standard deviation.

 $\rho_{\rm eff}$ value for particles emitted at 260 °C smoke. There temperature compared to those from 220 °C smoke. There was an increasing trend in $\rho_{\rm eff}$ observed for particles emitted at smoldering temperatures of both 220 and 260 °C until a V-TDMA volatilization temperature of 120 °C. Higher than this V-TDMA volatilization temperature, the average $\rho_{\rm eff}$ appeared to slightly decrease. The absence of data points between 60 and 250 °C makes it difficult to determine the maximum of the curve. This curve could imply some nonuniformity in the distribution of mass within the particles, or that the thermal volatilization process at higher temperatures is altering the chemical constituents. Nevertheless, the average $\rho_{\rm eff}$ values observed for the volatilization range were remarkably uniform.

In Figure 7, the MFR curve corresponding to particles emitted from 220 °C ignition decreases faster than those from 260 °C. At 120 °C volatilization temperature, particles emitted from 220 °C ignition had an MFR approaching 7%, while around 30% MFR was observed for particles emitted from 260 °C ignition. The initial diameters for both sets of particles were the same, approximately 200 nm. From this observation, we can qualitatively conclude that the organic materials constituting the nascent particles emitted at 220 °C ignition temperatures are more volatile in comparison to those emitted at 260 °C.

In conclusion, we show that the $\rho_{\rm eff}$ of BrC primary aerosols emitted from smoldering peat combustion are remarkably uniform as a function of particle size and volatile fraction removed. This constant value implies homogeneous internal composition for these particles and the absence of any coreshell type of internal structures, or if such a structure exists, that the core and shell materials have equal densities. This is the case even though condensing material is contributing to particle mass at the time of sampling, suggesting that condensing material is similar in density to the original particle material. The mass-mobility exponent of these particles was a constant 3.0, suggesting the morphology of these particles to be spherical, an observation consistent with previous work on spheres and tar balls from smoldering biomass burning both in laboratory settings and field studies. Future studies need to be conducted to investigate the effects of atmospheric processing on $\rho_{\rm eff}$ of these particles.

ASSOCIATED CONTENT

S Supporting Information

The Supporting Information is available free of charge on the ACS Publications website at DOI: 10.1021/acs.est.8b00093.

Details of our preliminary study of $\rho_{\rm eff}$ and MFR of volatilized BrC aerosols, XPS analysis of chemical composition of nascent aerosols, a description of the

IPN spectrometers, and the algorithm used to retrieve complex m (PDF)

AUTHOR INFORMATION

Corresponding Author

*Phone: (314) 935-6054; e-mail: chakrabarty@wustl.edu.

ORCID (

Benjamin J. Sumlin: 0000-0003-2909-7494 Rajan K. Chakrabarty: 0000-0001-5753-9937

Author Contributions

§B.J.S. and C.R.O. contributed equally to this work.

Notes

The authors declare no competing financial interest.

ACKNOWLEDGMENTS

This work was partially supported by the NSF under Grant Nos. AGS1455215 and CBET1437933, NASA ROSES under Grant No. NNX15AI66G, and the Consortium for Clean Coal Utilization (CCCU) at Washington University in St. Louis.

REFERENCES

- (1) Seinfeld, J. H.; Pandis, S. N. Atmos. Chem. Phys.: From Air Pollution to Climate Change; Wiley: 1998.
- (2) Liu, Y.; Daum, P. H. Relationship of refractive index to mass density and self-consistency of mixing rules for multicomponent mixtures like ambient aerosols. *J. Aerosol Sci.* **2008**, 39 (11), 974–986.
- (3) Fuchs, N. A. *The Mechanics of Aerosols*; Davies, C. N., Ed.; Macmillan, 1964; Translated from the Russian by Daisley, R. E.; Fuchs, M..
- (4) Park, K.; Cao, F.; Kittelson, D. B.; McMurry, P. H. Relationship between Particle Mass and Mobility for Diesel Exhaust Particles. *Environ. Sci. Technol.* **2003**, 37 (3), 577–583.
- (5) Bahreini, R.; Keywood, M. D.; Ng, N. L.; Varutbangkul, V.; Gao, S.; Flagan, R. C.; Seinfeld, J. H.; Worsnop, D. R.; Jimenez, J. L. Measurements of Secondary Organic Aerosol from Oxidation of Cycloalkenes, Terpenes, andm-Xylene Using an Aerodyne Aerosol Mass Spectrometer. *Environ. Sci. Technol.* **2005**, 39 (15), 5674–5688.
- (6) Alfarra, M. R.; Paulsen, D.; Gysel, M.; Garforth, A. A.; Dommen, J.; Prévôt, A. S. H.; Worsnop, D. R.; Baltensperger, U.; Coe, H. A mass spectrometric study of secondary organic aerosols formed from the photooxidation of anthropogenic and biogenic precursors in a reaction chamber. *Atmos. Chem. Phys.* **2006**, *6* (12), 5279–5293.
- (7) Olfert, J. S.; Symonds, J. P. R.; Collings, N. The effective density and fractal dimension of particles emitted from a light-duty diesel vehicle with a diesel oxidation catalyst. *J. Aerosol Sci.* **2007**, 38 (1), 69–82.
- (8) Johnson, T. J.; Symonds, J. P. R.; Olfert, J. S. Mass-Mobility Measurements Using a Centrifugal Particle Mass Analyzer and Differential Mobility Spectrometer. *Aerosol Sci. Technol.* **2013**, 47 (11), 1215–1225.
- (9) Ghazi, R.; Tjong, H.; Soewono, A.; Rogak, S. N.; Olfert, J. S. Mass, Mobility, Volatility, and Morphology of Soot Particles Generated by a McKenna and Inverted Burner. *Aerosol Sci. Technol.* **2013**, *47* (4), 395–405.
- (10) Skillas, G.; Künzel, S.; Burtscher, H.; Baltensperger, U.; Siegmann, K. High fractal-like dimension of diesel soot agglomerates. *J. Aerosol Sci.* **1998**, 29 (4), 411–419.
- (11) Schmidt-Ott, A.; Baltensperger, U.; Gäggeler, H. W.; Jost, D. T. Scaling behaviour of physical parameters describing agglomerates. *J. Aerosol Sci.* **1990**, 21 (6), 711–717.
- (12) McMurry, P. H.; Wang, X.; Park, K.; Ehara, K. The Relationship between Mass and Mobility for Atmospheric Particles: A New Technique for Measuring Particle Density. *Aerosol Sci. Technol.* **2002**, 36 (2), 227–238.

- (13) Momenimovahed, A.; Olfert, J. S. Effective Density and Volatility of Particles Emitted from Gasoline Direct Injection Vehicles and Implications for Particle Mass Measurement. Aerosol Sci. Technol. 2015, 49 (11), 1051-1062.
- (14) Olfert, J. S.; Collings, N. New method for particle mass classification—the Couette centrifugal particle mass analyzer. J. Aerosol Sci. 2005, 36 (11), 1338-1352.
- (15) Johnson, T. J.; Olfert, J. S.; Symonds, J. P. R.; Johnson, M.; Rindlisbacher, T.; Swanson, J. J.; Boies, A. M.; Thomson, K.; Smallwood, G.; Walters, D.; Sevcenco, Y.; Crayford, A.; Dastanpour, R.; Rogak, S. N.; Durdina, L.; Bahk, Y. K.; Brem, B.; Wang, J. Effective Density and Mass-Mobility Exponent of Aircraft Turbine Particulate Matter. J. Propul. Power 2015, 31 (2), 573-582.
- (16) Chakrabarty, R. K.; Gyawali, M.; Yatavelli, R. L. N.; Pandey, A.; Watts, A. C.; Knue, J.; Chen, L. W. A.; Pattison, R. R.; Tsibart, A.; Samburova, V.; Moosmuller, H. Brown carbon aerosols from burning of boreal peatlands: microphysical properties, emission factors, and implications for direct radiative forcing. Atmos. Chem. Phys. 2016, 16 (5), 3033-3040.
- (17) Chakrabarty, R.; Moosmüller, H.; Chen, L.-W.; Lewis, K.; Arnott, W.; Mazzoleni, C.; Dubey, M.; Wold, C.; Hao, W.; Kreidenweis, S. Brown carbon in tar balls from smoldering biomass combustion. Atmos. Chem. Phys. 2010, 10 (13), 6363-6370.
- (18) Turetsky, M. R.; Benscoter, B.; Page, S.; Rein, G.; van der Werf, G. R.; Watts, A. Global vulnerability of peatlands to fire and carbon loss. Nat. Geosci. 2014, 8 (1), 11-14.
- (19) Rein, G.; Cleaver, N.; Ashton, C.; Pironi, P.; Torero, J. L. The severity of smouldering peat fires and damage to the forest soil. Catena 2008, 74 (3), 304-309.
- (20) Balshi, M. S.; McGuire, A. D.; Duffy, P.; Flannigan, M.; Kicklighter, D. W.; Melillo, J. Vulnerability of carbon storage in North American boreal forests to wildfires during the 21st century. Global Change Biology 2009, 15 (6), 1491-1510.
- (21) Hu, F. S.; Higuera, P. E.; Walsh, J. E.; Chapman, W. L.; Duffy, P. A.; Brubaker, L. B.; Chipman, M. L. Tundra burning in Alaska: Linkages to climatic change and sea ice retreat. J. Geophys. Res. 2010, 115 (G4), G04002.
- (22) Oris, F.; Asselin, H.; Ali, A. A.; Finsinger, W.; Bergeron, Y. Effect of increased fire activity on global warming in the boreal forest. Environ. Rev. 2014, 22 (3), 206-219.
- (23) Randerson, J. T.; Liu, H.; Flanner, M. G.; Chambers, S. D.; Jin, Y.; Hess, P. G.; Pfister, G.; Mack, M. C.; Treseder, K. K.; Welp, L. R.; Chapin, F. S.; Harden, J. W.; Goulden, M. L.; Lyons, E.; Neff, J. C.; Schuur, E. A. G.; Zender, C. S. The Impact of Boreal Forest Fire on Climate Warming. Science 2006, 314 (5802), 1130-1132.
- (24) Chen, Y.; Bond, T. Light absorption by organic carbon from wood combustion. Atmos. Chem. Phys. 2010, 10 (4), 1773-1787.
- (25) Feng, Y.; Ramanathan, V.; Kotamarthi, V. Brown carbon: a significant atmospheric absorber of solar radiation? Atmos. Chem. Phys. 2013, 13 (17), 8607-8621.
- (26) Jo, D. S.; Park, R. J.; Lee, S.; Kim, S. W.; Zhang, X. L. A global simulation of brown carbon: implications for photochemistry and direct radiative effect. Atmos. Chem. Phys. 2016, 16 (5), 3413-3432.
- (27) Liu, J.; Scheuer, E.; Dibb, J.; Diskin, G. S.; Ziemba, L. D.; Thornhill, K. L.; Anderson, B. E.; Wisthaler, A.; Mikoviny, T.; Devi, J. J.; Bergin, M.; Perring, A. E.; Markovic, M. Z.; Schwarz, J. P.; Campuzano-Jost, P.; Day, D. A.; Jimenez, J. L.; Weber, R. J. Brown carbon aerosol in the North American continental troposphere: sources, abundance, and radiative forcing. Atmos. Chem. Phys. 2015, 15 (14), 7841 - 7858.
- (28) Chung, C. E.; Ramanathan, V.; Decremer, D. Observationally constrained estimates of carbonaceous aerosol radiative forcing. Proc. Natl. Acad. Sci. U. S. A. 2012, 109 (29), 11624-11629.
- (29) Saleh, R.; Marks, M.; Heo, J.; Adams, P. J.; Donahue, N. M.; Robinson, A. L. Contribution of brown carbon and lensing to the direct radiative effect of carbonaceous aerosols from biomass and biofuel burning emissions. J. Geophys. Res.: Atmos. 2015, 120 (19), 10285-10296.

- (30) Andreae, M.; Gelencsér, A. Black carbon or brown carbon? The nature of light-absorbing carbonaceous aerosols. Atmos. Chem. Phys. **2006**, 6 (10), 3131–3148.
- (31) Bond, T. C.; Bergstrom, R. W. Light Absorption by Carbonaceous Particles: An Investigative Review. Aerosol Sci. Technol. 2006, 40 (1), 27-67.
- (32) Petzold, A.; Ogren, J. A.; Fiebig, M.; Laj, P.; Li, S. M.; Baltensperger, U.; Holzer-Popp, T.; Kinne, S.; Pappalardo, G.; Sugimoto, N.; Wehrli, C.; Wiedensohler, A.; Zhang, X. Y. Recommendations for reporting "black carbon" measurements. Atmos. Chem. Phys. 2013, 13 (16), 8365-8379.
- (33) Sun, H.; Biedermann, L.; Bond, T. C. Color of brown carbon: A model for ultraviolet and visible light absorption by organic carbon aerosol. Geophys. Res. Lett. 2007, 34 (17), L17813.
- (34) Laskin, A.; Laskin, J.; Nizkorodov, S. A. Chemistry of Atmospheric Brown Carbon. Chem. Rev. 2015, 115 (10), 4335-4382.
- (35) Tóth, A.; Hoffer, A.; Nyirő-Kósa, I.; Pósfai, M.; Gelencsér, A. Atmospheric tar balls: aged primary droplets from biomass burning? Atmos. Chem. Phys. 2014, 14 (13), 6669-6675.
- (36) Dinar, E.; Mentel, T. F.; Rudich, Y. The density of humic acids and humic like substances (HULIS) from fresh and aged wood burning and pollution aerosol particles. Atmos. Chem. Phys. Discuss. **2006**, 6 (4), 7835–7867.
- (37) Hoffer, A.; Gelencsér, A.; Guyon, P.; Kiss, G.; Schmid, O.; Frank, G. P.; Artaxo, P.; Andreae, M. O. Optical properties of humiclike substances (HULIS) in biomass-burning aerosols. Atmos. Chem. Phys. 2006, 6 (11), 3563-3570.
- (38) Simpson, I. J.; Akagi, S. K.; Barletta, B.; Blake, N. J.; Choi, Y.; Diskin, G. S.; Fried, A.; Fuelberg, H. E.; Meinardi, S.; Rowland, F. S.; Vay, S. A.; Weinheimer, A. J.; Wennberg, P. O.; Wiebring, P.; Wisthaler, A.; Yang, M.; Yokelson, R. J.; Blake, D. R. Boreal forest fire emissions in fresh Canadian smoke plumes: C₁-C₁₀ volatile organic compounds (VOCs), CO₂, CO, NO₂, NO, HCN and CH₃CN. Atmos. Chem. Phys. 2011, 11 (13), 6445-6463.
- (39) Huijnen, V.; Williams, J.; van Weele, M.; van Noije, T.; Krol, M.; Dentener, F.; Segers, A.; Houweling, S.; Peters, W.; de Laat, J.; Boersma, F.; Bergamaschi, P.; van Velthoven, P.; Le Sager, P.; Eskes, H.; Alkemade, F.; Scheele, R.; Nédélec, P.; Pätz, H. W. The global chemistry transport model TM5: description and evaluation of the tropospheric chemistry version 3.0. Geosci. Model Dev. 2010, 3 (2), 445-473.
- (40) Canagaratna, M. R.; Jimenez, J. L.; Kroll, J. H.; Chen, Q.; Kessler, S. H.; Massoli, P.; Hildebrandt Ruiz, L.; Fortner, E.; Williams, L. R.; Wilson, K. R.; Surratt, J. D.; Donahue, N. M.; Jayne, J. T.; Worsnop, D. R. Elemental ratio measurements of organic compounds using aerosol mass spectrometry: characterization, improved calibration, and implications. Atmos. Chem. Phys. 2015, 15 (1), 253-272.
- (41) Maricq, M. M.; Xu, N.; Chase, R. E. Measuring Particulate Mass Emissions with the Electrical Low Pressure Impactor. Aerosol Sci. Technol. 2006, 40 (1), 68-79.
- (42) Usup, A.; Hashimoto, Y.; Takahashi, H.; Hayasaka, H. Combustion and thermal characteristics of peat fire in tropical peatland in Central Kalimantan, Indonesia. Tropics 2004, 14 (1), 1-19.
- (43) Wiedensohler, A.; Birmili, W.; Nowak, A.; Sonntag, A.; Weinhold, K.; Merkel, M.; Wehner, B.; Tuch, T.; Pfeifer, S.; Fiebig, M.; Fjäraa, A. M.; Asmi, E.; Sellegri, K.; Depuy, R.; Venzac, H.; Villani, P.; Laj, P.; Aalto, P.; Ogren, J. A.; Swietlicki, E.; Williams, P.; Roldin, P.; Quincey, P.; Hüglin, C.; Fierz-Schmidhauser, R.; Gysel, M.; Weingartner, E.; Riccobono, F.; Santos, S.; Grüning, C.; Faloon, K.; Beddows, D.; Harrison, R.; Monahan, C.; Jennings, S. G.; O'Dowd, C. D.; Marinoni, A.; Horn, H. G.; Keck, L.; Jiang, J.; Scheckman, J.; McMurry, P. H.; Deng, Z.; Zhao, C. S.; Moerman, M.; Henzing, B.; de Leeuw, G.; Löschau, G.; Bastian, S. Mobility particle size spectrometers: harmonization of technical standards and data structure to facilitate high quality long-term observations of atmospheric particle number size distributions. Atmos. Meas. Tech. 2012, 5 (3), 657-685.
- (44) Sumlin, B. J.; Heinson, W. R.; Chakrabarty, R. K. Retrieving the aerosol complex refractive index using PyMieScatt: A Mie computa-

- tional package with visualization capabilities. *J. Quant. Spectrosc. Radiat. Transfer* **2018**, 205, 127–134.
- (45) Zhang, S.-H.; Seifeld, J. H.; Flagan, R. C. Determination of Particle Vapor Pressures Using the Tandem Differential Mobility Analyzer. *Aerosol Sci. Technol.* **1993**, *19* (1), 3–14.
- (46) Philippin, S.; Wiedensohler, A.; Stratmann, F. Measurements of non-volatile fractions of pollution aerosols with an eight-tube volatility tandem differential mobility analyzer (VTDMA-8). *J. Aerosol Sci.* **2004**, 35 (2), 185–203.
- (47) Sumlin, B. J.; Heinson, Y. W.; Shetty, N.; Pandey, A.; Pattison, R. S.; Baker, S.; Hao, W. M.; Chakrabarty, R. K. UV-Vis-IR spectral complex refractive indices and optical properties of brown carbon aerosol from biomass burning. *J. Quant. Spectrosc. Radiat. Transfer* **2018**, 206, 392–398.
- (48) Sumlin, B. J.; Pandey, A.; Walker, M. J.; Pattison, R. S.; Williams, B. J.; Chakrabarty, R. K. Atmospheric Photooxidation Diminishes Light Absorption by Primary Brown Carbon Aerosol from Biomass Burning. *Environ. Sci. Technol. Lett.* **2017**, 4 (12), 540–545.
- (49) Lambe, A. T.; Cappa, C. D.; Massoli, P.; Onasch, T. B.; Forestieri, S. D.; Martin, A. T.; Cummings, M. J.; Croasdale, D. R.; Brune, W. H.; Worsnop, D. R.; Davidovits, P. Relationship between Oxidation Level and Optical Properties of Secondary Organic Aerosol. *Environ. Sci. Technol.* **2013**, 47 (12), 6349–6357.
- (50) Pósfai, M.; Gelencsér, A.; Simonics, R.; Arató, K.; Li, J.; Hobbs, P. V.; Buseck, P. R. Atmospheric tar balls: Particles from biomass and biofuel burning. *J. Geophys. Res.: Atmos.* **2004**, *109* (D6), D06213.
- (51) China, S.; Mazzoleni, C.; Gorkowski, K.; Aiken, A. C.; Dubey, M. K. Morphology and mixing state of individual freshly emitted wildfire carbonaceous particles. *Nat. Commun.* **2013**, *4*, 2122.
- (52) Pósfai, M.; Simonics, R.; Li, J.; Hobbs, P. V.; Buseck, P. R. Individual aerosol particles from biomass burning in southern Africa: 1. Compositions and size distributions of carbonaceous particles. *J. Geophys. Res.: Atmos.* **2003**, *108* (D13), 8483.
- (53) Tivanski, A. V.; Hopkins, R. J.; Tyliszczak, T.; Gilles, M. K. Oxygenated Interface on Biomass Burn Tar Balls Determined by Single Particle Scanning Transmission X-ray Microscopy. *J. Phys. Chem. A* **2007**, 111 (25), 5448–5458.
- (54) Kumar, P.; Fennell, P.; Britter, R. Effect of wind direction and speed on the dispersion of nucleation and accumulation mode particles in an urban street canyon. *Sci. Total Environ.* **2008**, *402* (1), 82–94.
- (55) Gouriou, F.; Morin, J. P.; Weill, M. E. On-road measurements of particle number concentrations and size distributions in urban and tunnel environments. *Atmos. Environ.* **2004**, *38* (18), 2831–2840.
- (56) Roth, E.; Kehrli, D.; Bonnot, K.; Trouvé, G. Size distributions of fine and ultrafine particles in the city of Strasbourg: Correlation between number of particles and concentrations of NOx and SO2 gases and some soluble ions concentration determination. *J. Environ. Manage.* 2008, 86 (1), 282–290.
- (57) Maricq, M. M.; Xu, N. The effective density and fractal dimension of soot particles from premixed flames and motor vehicle exhaust. *J. Aerosol Sci.* **2004**, *35* (10), 1251–1274.
- (58) Zelenyuk, A.; Cai, Y.; Imre, D. From Agglomerates of Spheres to Irregularly Shaped Particles: Determination of Dynamic Shape Factors from Measurements of Mobility and Vacuum Aerodynamic Diameters. *Aerosol Sci. Technol.* **2006**, *40* (3), 197–217.
- (59) Rein, G. Smouldering Combustion Phenomena in Science and Technology. Int. Rev. Chem. Eng. 2009, 1, 3–18.